

Flexible High-Performance and Solution-Processed Organic Photovoltaics with Robust Mechanical Stability

Yanna Sun, Lingxian Meng, Xiangjian Wan, Ziqi Guo, Xin Ke, Zhenhe Sun, Kai Zhao, Hongtao Zhang, Chenxi Li, and Yongsheng Chen*

Among the various advantages of organic photovoltaics (OPVs), the key one is their ability to be a highly flexible renewable energy source. However, the power conversion efficiencies for flexible OPV devices still lag behind those of their rigid counterparts, and their mechanical stability cannot meet the requirements for practical applications at present. These, in particular, depend on flexible transparent electrodes (FTEs). Here, a high-quality FTE (called FlexAgNE), with the simultaneously combined excellent characteristics, has been tested with a series of efficient active materials for flexible OPV devices, and high performance comparable with rigid counterparts has been achieved. In addition, due to the synergistic effect of FlexAgNE and the upper ZnO transport layer, including strong binding between the polyethylene terephthalate substrate and a hydrophilic polyelectrolyte (the key component of FlexAgNE), together with the capillary force effect of crossed silver nanowires and tight filling of ZnO, the flexible devices demonstrate robust mechanical stability even under extreme bending or folding conditions.

smoothness, mechanical flexibility and etc. Among various FTE materials such as conducting polymers, carbon nanotubes, graphene, metallic nanowires, and ultrathin metal,^[25,27–37] silver nanowire (AgNW) is considered as one of the most promising candidates due to its good conductivity, high transmittance, excellent mechanical flexibility, and easy solution processability.^[18,25,38]

In the past few years, great efforts have focused on designing high-quality AgNWs-based FTEs suitable for flexible OPV devices,^[18,25,39] mainly with an inverted device structure due to its compatibility with future commercial applications along with the generally more stable performance. Recently, utilizing an ionic electrostatic charge repulsion strategy via introducing a polyelectrolyte into an AgNWs-water suspension, we have reported a high-quality FTE

(called FlexAgNE) and further demonstrated high-performance flexible OPV devices with a series of different donor and acceptor materials.^[25] Thus, the flexible single-junction and tandem devices achieved impressive PCEs of 13.1% and 16.5%, respectively, highly comparable to those of rigid counterparts. Also, these flexible OPV devices have demonstrated excellent mechanical flexibility/stability.^[25] These results indicate that FlexAgNE holds great promise as a superior FTE in high-efficiency systems. Note OPV area has witnessed a great step forward in the last few years mainly due to the newly emerging star acceptor Y6 and its derivatives, and the rigid devices have demonstrated outstanding device performance of over 17%.^[9,10,13–17] Thus, it is natural and important to study the performance of flexible OPV devices with these outstanding new materials. Indeed, a few explorations have been made with Y6 and its derivatives for flexible devices and PCEs of 14–16% have been reported.^[18,20,23] In these works, FTEs were fabricated with different approaches, including embedding AgNWs in UV-curing resin and film transferring of AgNWs films coated with polystyrene (PS) spheres. Given the above results, to simplify the process, we feel it is important to explore whether our FlexAgNEs, available with an easy one-step water solution process, can be successfully applied with the new and efficient Y6 and its derivative material systems for high-performance flexible devices.

Regarding mechanical flexibility/stability, it is particularly important for flexible OPVs when used in practical applications, of which the key is the flexibility of FTE.^[18–20,26] To increase the compatibility with roll-to-roll production, fabricating mechanically robust FTEs through fully solution-processed approach is

1. Introduction

Organic photovoltaics (OPVs) have attracted considerable attention owing to their unique advantages of lightweight, low cost, large-area printing fabrication, and mechanical flexibility.^[1–8] Recently, power conversion efficiencies (PCEs) of over 17% have been achieved for rigid single-junction OPV devices with the conventional device structure (versus general lower PCEs when using the inverted structure).^[9–17] Noting that the flexibility is the most distinguishing characteristic for OPVs that outweighs the inorganic photovoltaic technologies based on crystal-silicon and other thin films.^[18–21] As the key component, flexible transparent electrode (FTE) plays a decisive role in flexible device performance.^[22–26] High-quality FTEs should simultaneously possess excellent opto-electrical properties, film uniformity, surface

Y. Sun, L. Meng, Prof. X. Wan, Z. Guo, X. Ke, Z. Sun, K. Zhao, Dr. H. Zhang, Prof. C. Li, Prof. Y. Chen
State Key Laboratory and Institute of Elemento-Organic Chemistry
The Centre of Nanoscale Science and Technology and
Key Laboratory of Functional Polymer Materials
Renewable Energy Conversion and Storage Center (RECAST)
College of Chemistry
Nankai University
Tianjin 300071, China
E-mail: yschen99@nankai.edu.cn

 The ORCID identification number(s) for the author(s) of this article can be found under <https://doi.org/10.1002/adfm.202010000>.

DOI: 10.1002/adfm.202010000

also highly desirable. In addition, though AgNWs-based FTEs have been widely studied, previous works mainly focused on the performance, such as opto-electrical property, surface smoothness, and flexibility.^[38,40–43] However, so far, there has been little discussion about the mechanism underlying the superior mechanical robustness of AgNWs-based FTEs. Note that the underlining mechanical robustness should include the entire FTEs, that is, all the components and the binding/connection of all these components. Hence, a comprehensive understanding of the mechanism is also urgently required for future better design of mechanically robust AgNWs-based FTEs.

In this work, based on our high-quality FlexAgNEs,^[25] flexible OPV devices have been fabricated and studied with the current star acceptor Y6 and its derivatives. Importantly, comparable performance with rigid counterparts has been achieved for all the tested materials. In particular, the flexible single-junction devices have offered a high PCE of 15.60%. In addition, flexible devices display superior and robust mechanical stability even under extreme bending or folding conditions. Furthermore, the mechanism underlying the superior mechanical robustness of these flexible devices has been thoroughly investigated, which is mainly attributed to the synergistic effect of FlexAgNE and the upper ZnO transport layer. Specifically, for FlexAgNE, strong interaction of the hydrophilic polyelectrolyte with ozone-treated polyethylene terephthalate (PET) substrate contributes to the observed robust mechanical adhesion. Besides, the capillary force effect of the crossed AgNWs junction and tight filling of ZnO in the grid-like AgNWs network leads to a strong bonding of AgNWs to substrate, which also reduces the impact of brittle ZnO on flexibility. This comprehensive understanding would guide future FTEs design to realize higher and more mechanically stable performance for flexible organic electronics.

2. Results and Discussion

With this high-quality FlexAgNE, flexible OPV devices were fabricated and studied with several typical Y6 and its derivatives using an inverted device structure (Figure 1a). These materials, commercially available, were selected because they exhibit currently the best performance in the rigid devices.^[11,12,44] The detailed fabrication process is described in Supporting Information. As depicted in Figure 1b, the work function of FlexAgNE/ZnO (−4.33 eV) is comparable to that of ITO/ZnO (−4.30 eV), indicating that the charge carriers could be injected equally into FlexAgNE/ZnO and ITO/ZnO (Figure S1, Supporting Information). Also, the energy level of FlexAgNE/ZnO matched very well with these active materials, which is beneficial for charge collection of the FlexAgNEs.

The current density versus voltage (J – V) curves of these flexible devices and the corresponding rigid devices were characterized and compared as presented in Figure 1c and Figure S2a,c, Supporting Information. The photovoltaic parameters of these corresponding devices are summarized in Table 1. The above results demonstrated that high performance was successfully achieved for flexible OPV devices based on these typical Y6-system materials (PM6:BTP-4F-12, PM6:Y6:PC₆₁BM, and PM6:Y6), which was highly comparable to those of the rigid counterparts. This is consistent with our previous report (as shown in Table S1, Supporting Information),^[25] demonstrating that our easily accessible

FlexAgNEs could also work well for these new material systems. For example, the flexible single-junction devices based on PM6:BTP-4F-12 offered a high PCE of 15.60% with open circuit voltage (V_{oc}), short circuit current density (J_{sc}), and fill factor (FF) of 0.837 V, 24.92 mA cm^{−2}, and 74.8%, respectively. The efficiency histograms of PM6:BTP-4F-12-based flexible devices is shown in Figure 1c. Apparently, the flexible devices exhibited a narrowed distribution of PCEs, demonstrating a good reproducibility for the flexible devices based on our FlexAgNEs. Among these photovoltaic parameters, the same V_{oc} for flexible devices and rigid counterparts is attributed to the similar work function of FlexAgNE/ZnO and ITO/ZnO (Figure S1, Supporting Information). Besides, outstanding FF values over 74% have been achieved for these flexible devices, indicating negligible leakage current but high rectification ratio of FlexAgNE, which is attributed to its favorable grid-like pattern and smooth surface morphology^[25] (as shown in Figure S4, Supporting Information). In addition, the J_{sc} values were also confirmed by the corresponding external quantum efficiency (EQE) measurements shown in Figure 1d and Figure S2b,d, Supporting Information. The EQE spectrum of the glass/ITO-based reference device has higher values in the wavelength range from 450 to 600 nm compared with the PET/FlexAgNE-based flexible device. These results can be attributed to the high absorption of the PET/FlexAgNE in the short-wavelength region, reducing the light absorption of the active layer. Besides, the value and pattern of EQE spectrum for different blends are consistent with the absorption spectra of the rigid counterparts, which are in agreement with our previous results^[25] (Figure S3, Supporting Information). All these together make these flexible OPV devices based on FlexAgNEs with Y6 and its derivative systems achieve excellent and comparable performance with rigid counterparts.

Large-area device performance is of vital importance for flexible devices being used in practical applications. Based on the results discussed above at small area for the flexible devices, large-area flexible devices (1 cm²) were further fabricated and studied. As shown in Table S2, Supporting Information, these devices with area of 1 cm² also exhibit comparable performance to those of the rigid devices. Note such a large-area flexible device based on PM6:BTP-4F-12 yields an outstanding PCE of 12.86%, which is the highest PCE reported for large-area flexible OPVs so far.^[18] These results indicate that from small-area to large-scale devices, the performance is well maintained for devices based on our FlexAgNEs, mainly ascribing to all the combined excellent characteristics together for FlexAgNEs, including the high conductivity, appropriate work function, and smooth surface.^[25,45] Overall, the above results clearly demonstrated that FlexAgNEs can be successfully applied with the recently emerging efficient star acceptor Y6 and its derivative systems for high-performance flexible devices.

With high performance of the relatively large-area flexible devices, the device stability has been further studied. As shown in Figure S5, Supporting Information, all the tested flexible devices show rather high stability and small degradations, with <5% of their initial values in terms of PCEs after testing over 170 days. Note these stability results of flexible devices are similar to those of the corresponding rigid devices. Thus, FlexAgNE does not lead to obvious PCE degradation, suggesting FlexAgNE could be a promising candidate for future large-scale production of flexible and stable organic electronics.

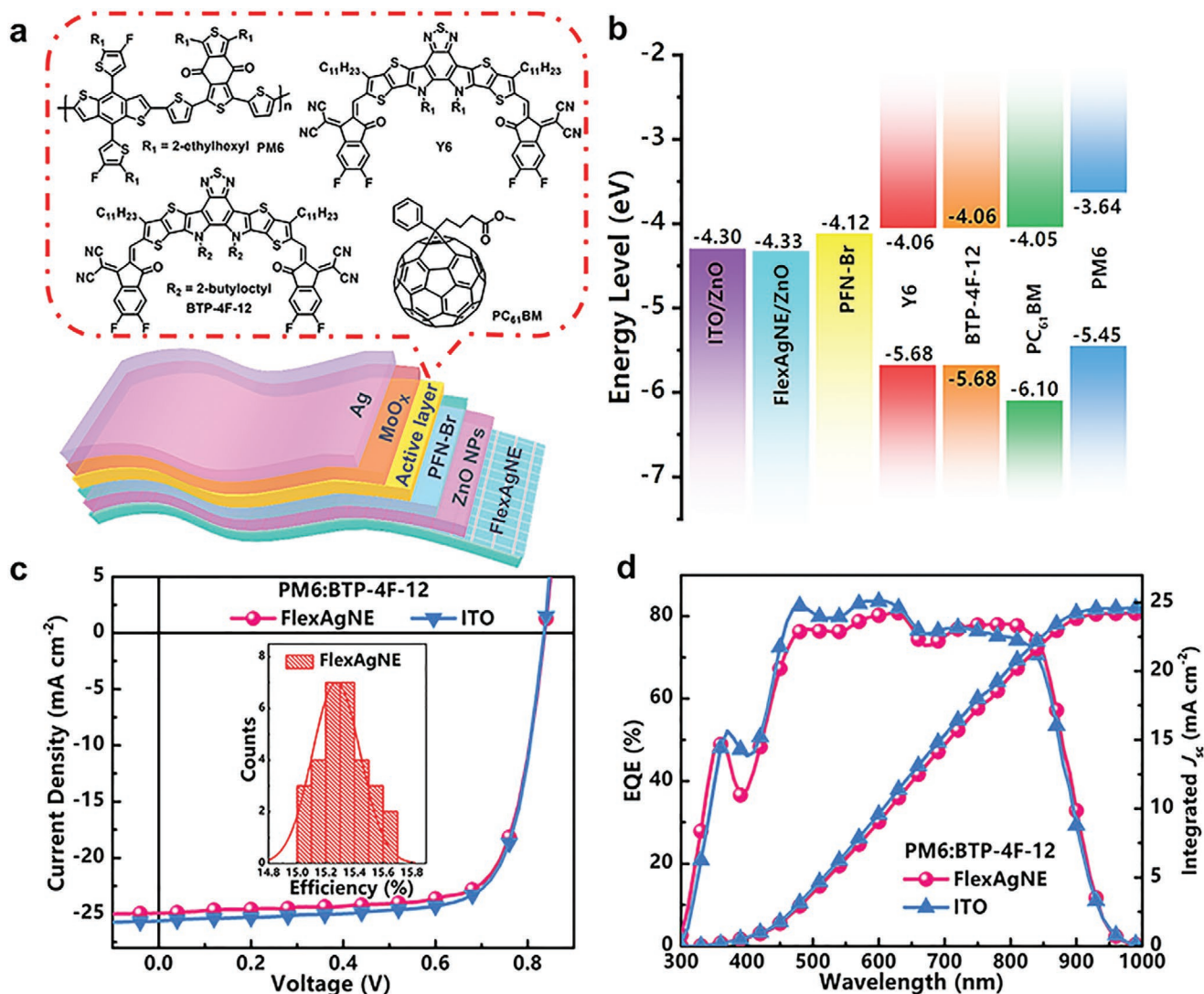


Figure 1. a) Schematic of flexible OPV devices and molecular structures of PM6, Y6, BTP-4F-12, and PC₆₁BM in active layers. b) Energy level diagram. c) J-V curves of a typical device (PM6:BTP-4F-12) based on FlexAgNEs and rigid ITO electrodes; the inset shows the histograms of PCE from 30 flexible devices based on PM6:BTP-4F-12 blend. d) EQE spectra and the integrated J_{sc} of a typical device (PM6:BTP-4F-12) based on FlexAgNEs and rigid ITO electrodes.

With excellent performance of these flexible OPV devices, the mechanical flexibility with bending tests both in inward and outward directions was tested for one typical system of PM6:BTP-4F-12 (Figure 2a). Relative photovoltaic parameters decay of the flexible device as a function of bending cycles at

a radius of 3 mm were presented in Figure 2b and Figure S5, Supporting Information. After total continuous 1000 bending cycles, the degradation of V_{oc} was negligible (below 1%), and J_{sc} and FF also still maintained over 96% and 94% of their initial values (Figure S6, Supporting Information). Thus,

Table 1. Photovoltaic parameters of the OPV devices based on FlexAgNEs and rigid ITO electrodes with several typical Y6 and its derivative material systems.

Active layer	Electrode	V _{oc} [V]	J _{sc} [mA cm ⁻²]	FF [%]	PCE _{max} (PCE _{ave}) [%] ^a
PM6:BTP-4F-12	FlexAgNE	0.837	24.92	74.8	15.60 (15.28)
	ITO	0.837	25.60	74.7	16.01 (15.74)
PM6:Y6:PC ₆₁ BM	FlexAgNE	0.837	24.70	74.5	15.40 (15.08)
	ITO	0.837	25.54	74.8	15.99 (15.69)
PM6:Y6	FlexAgNE	0.829	24.87	74.3	15.32 (14.89)
	ITO	0.829	25.43	74.5	15.71 (15.43)

^aThe average PCE values were calculated from 10 devices and the area of the devices is ≈4 mm².

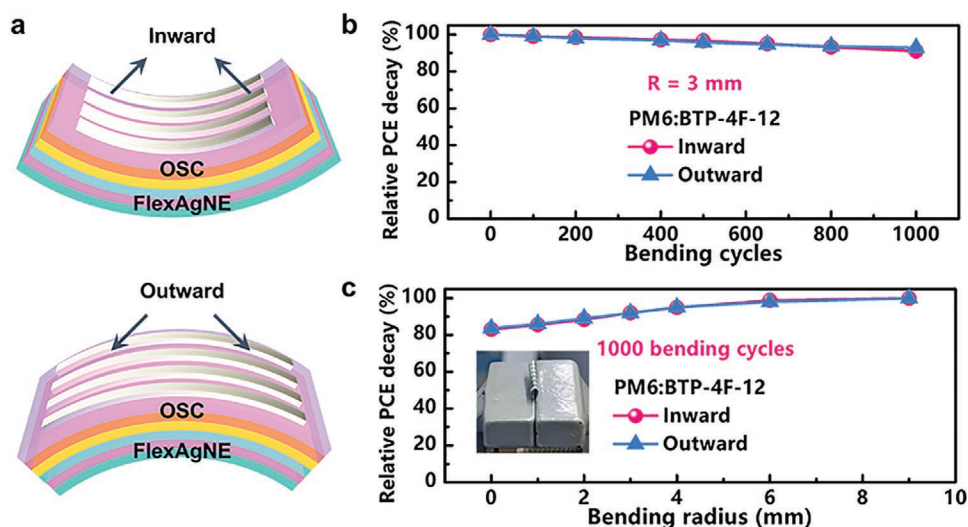


Figure 2. a) Schematics of inward and outward bending tests. b) Relative PCE decay for flexible OPV devices as a function of bending cycles ($R = 3$ mm). c) Relative PCE decay for flexible OPV devices as function of various bending radius (0–9 mm) after 1000 bending cycles.

PCEs retention of 91% and 93% were achieved in inward and outward bending directions, respectively (Figure 2b). The slightly reduced J_{sc} and FF might be due to the increased resistance and charge carrier recombination for flexible devices after bending. Considering that the mechanical flexibility of the active layer may be affected by the interfacial adhesion,^[46] to confirm the role of the PFN-Br layer, the mechanical flexibility of flexible devices without PFN-Br based on a typical PM6:BTP-4F-12 active layer was further tested (Figure S7, Supporting Information). After total continuous 1000 bending cycles ($R = 3$ mm), the PCEs of flexible devices without PFN-Br still retained 90% and 93% of the initial efficiencies in inward and outward bending directions. These results are very similar to those of the devices with PFN-Br (retentions of 91% and 93%), indicating the mechanical reliability of active layer was not affected by the PFN-Br.

High mechanical stability under extreme bending or even completely folding conditions for flexible OPV devices plays a key role in long-time or cyclic use such as wearable devices, which was further evaluated as depicted in Figure 2c. After 1000 bending cycles, the PCEs of flexible devices maintained well at various bending radius (0–9 mm), and even with > 83% PCEs retention at bending radius close to 0 mm in both bending directions. These results indicated that FlexAgNEs possess rather robust mechanical stability, which is consistent with its undamaged film morphology and the entire electrode structure after bending as discussed below.

To further understand the origin of the mechanical flexibility/stability of these flexible devices, morphology changes for different functional layers and the entire electrode structure after 1000 bending cycles were investigated by scanning electron microscopy (SEM). As shown in Figure 3a–f, very few cracks are visible for FlexAgNE/ZnO and with the upper active layer (PM6:BTP-4F-12), implying that these functional layers offer superior mechanical robustness in both directions. But after depositing with the top Ag electrode for complete flexible devices, clear small cracks can be found from the top

Ag electrodes after 1000 bending cycles (Figure 3g,h). Thus, the slightly degraded OPV performance after bending for the flexible devices as shown in Figure 2b,c is probably due to the geometrical cracks (defects) of top Ag electrodes, not from the FlexAgNE or FlexAgNE/ZnO layers.

To investigate the origin of the excellent mechanical robustness of FlexAgNE and FlexAgNE/ZnO, surface SEM images of PET/AgNWs and PET/AgNWs/ZnO films without the poly(sodium 4-styrenesulfonate) (PSSNa) were characterized after high cyclic bending as a reference. As shown in Figure 4a,b, the red dotted box exhibits clear AgNWs fracture and deep cracks of the ZnO film, which is significantly different from the unchanged morphology for FlexAgNE and FlexAgNE/ZnO layers (Figure 3a–d). These results are well consistent with the corresponding cross-sectional SEM images (Figure 4c–f). As shown in Figure 4c, the top AgNWs are more likely to be broken after bending, which is probably caused by the large stresses for the top AgNWs in the solvent evaporating and film formation process. Besides, large holes and cracks are found in the PET/AgNWs/ZnO layers (Figure 4d) with the loose ZnO nanoparticles in aggregated AgNWs. In contrast, no damage is observed for FlexAgNE and FlexAgNE/ZnO layers via introducing PSSNa (Figure 4e,f). For this different phenomenon in PET/AgNWs and FlexAgNE, the possible reasons were proposed as follows. 1) After adding PSSNa to AgNWs suspension, PSS anions were adsorbed on the AgNWs surface. 2) For FlexAgNE, due to electrostatic repulsion from PSS ions, AgNWs could be kept uniformly dispersed during the film preparation process (Figure 4e). 3) The grid-like AgNWs in close contact is favorable for forming a tight ZnO film above it. In addition, considering the amphoteric nature of ZnO, this should lead to the ionic interaction between ZnO and PSS anions, which will eventually improve the reliability of the FlexAgNE/ZnO. With these, FlexAgNE/ZnO ultimately achieved a uniform and compact film, which exhibited better mechanical stability than PET/AgNWs/ZnO. To further analyze morphology changes for the interlayer space, focused ion beam (FIB)-SEM was performed (Figure 4g–j), in which

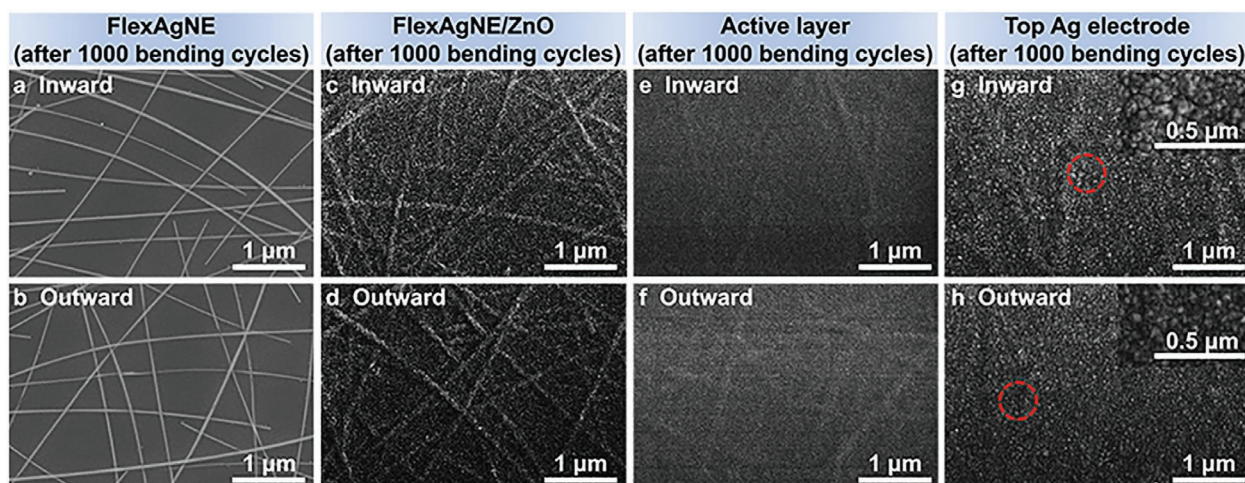


Figure 3. Surface SEM images of a,b) FlexAgNE, c,d) FlexAgNE/ZnO stacks, e,f) the active layer (PM6:BTP-4F-12) on top of FlexAgNE/ZnO/PFN-Br layers, and g,h) the Ag electrode on top of flexible devices after 1000 bending cycles in inward or outward bending directions ($R = 3$ mm). The red circles represent the small cracks from the top Ag electrodes after 1000 bending cycles, and the corresponding magnified images are shown in the inserted images (top right of graphs).

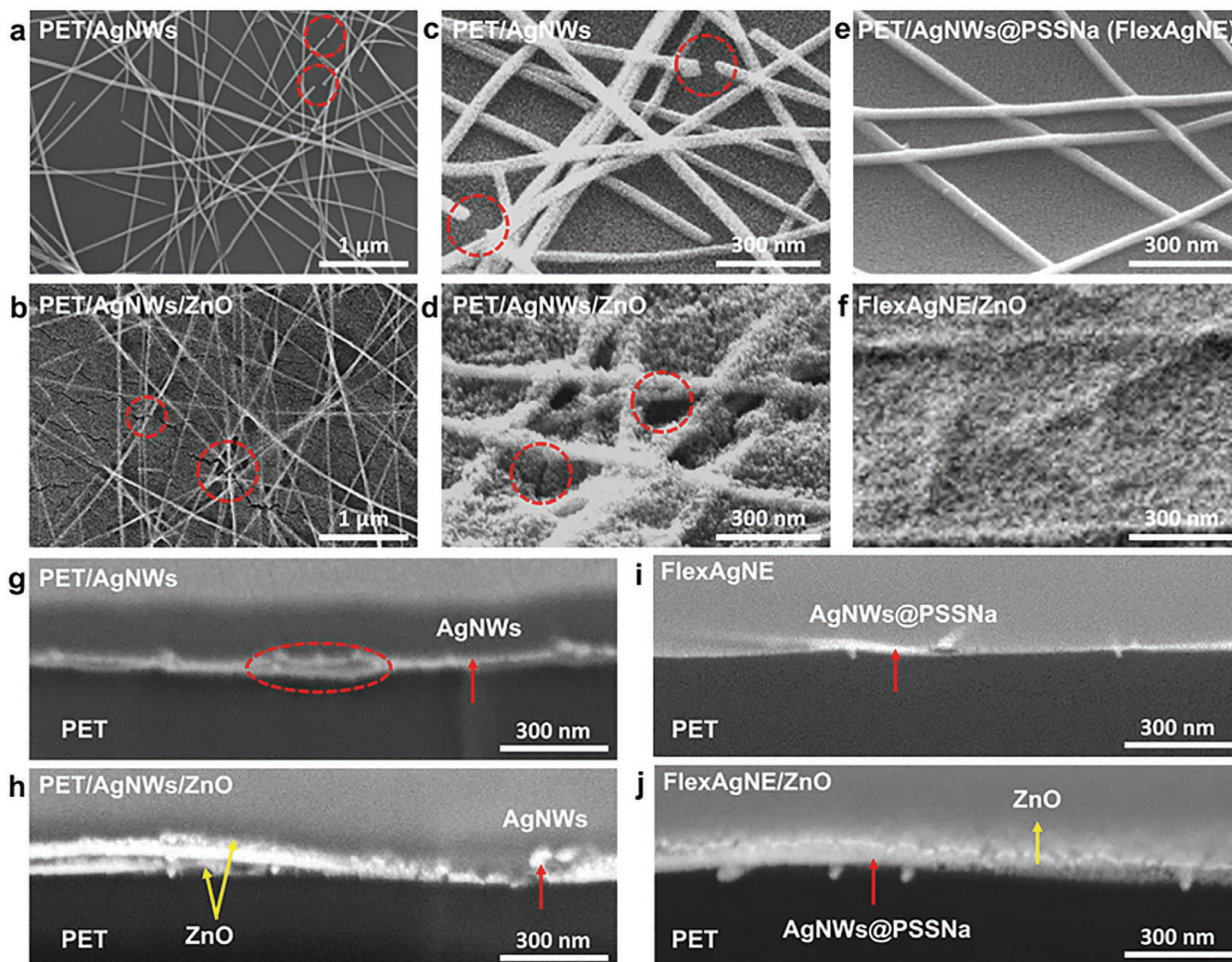


Figure 4. Surface SEM images of a) PET/AgNWs and b) PET/AgNWs/ZnO stacks, prepared without the poly(sodium 4-styrenesulfonate) (PSSNa), after 1000 bending cycles in inward direction. c–f) Cross-section SEM images and g–j) FIB-SEM images of c,g) PET/AgNWs, d,h) PET/AgNWs/ZnO stacks, e,i) PET/AgNWs@PSSNa (FlexAgNE, prepared with PSSNa), and f,j) FlexAgNE/ZnO stacks after 1000 bending cycles in inward direction ($R = 3$ mm). The red dotted boxes exhibit clear AgNWs fracture or deep cracks of the ZnO film. The arrows highlight the observed AgNWs (red) and ZnO (yellow) components, respectively.

all the components including PET, AgNWs, AgNWs@PSSNa, and ZnO, can be clearly observed. After 1000 bending cycles, while some shedding or loosening for both PET/AgNWs and PET/AgNWs/ZnO layers were found (Figure 4g,h), but neither delamination nor crack was observed for FlexAgNE or FlexAgNE/ZnO stacks. Furthermore, for PET/AgNWs, the AgNWs were easy to peel off with tape, which are prone to delamination and mechanical damage. In contrast, no obvious detachment for FlexAgNE and FlexAgNE/ZnO was observed in mechanical scratching adhesion test. Thus, the FlexAgNE and FlexAgNE/ZnO stacks were rated as level 1 according to the national standards from 1 to 7 of the adhesion tests (Figure S8, Supporting Information). Besides, the adhesive force for PET/AgNWs and PET/FlexAgNE was further analyzed. PET/AgNWs has a relatively low adhesion force of 0.02 mN, whereas the force for PET/FlexAgNE was dramatically increased to 0.1 mN. These results fully demonstrate that both FlexAgNE and FlexAgNE/ZnO exhibit strong adhesion together with superior mechanical robustness, which is essential for high-performance flexible electrode and organic electronics.

The mechanism underlying the superior mechanical robustness of FlexAgNE and FlexAgNE/ZnO stacks was thoroughly investigated, which is mainly attributed to the synergistic effect of FlexAgNE and the upper ZnO transport layer. Possible mechanism is offered in Figure 5a and summarized below: for FlexAgNE, the hydrogen bond and van der Waals bond would form between the ozone-treated PET substrate and the hydrophilic polyelectrolyte (PSSNa). The binding force was generated from the interactions between sulfonic groups of PSSNa and hydroxyl groups of ozone-treated PET. These intermolecular forces would

provide a strong adhesion interface.^[47,48] In addition, with evaporation of water, the capillary force effect would occur at the crossed AgNWs junctions during film formation process, which could tightly bind the crossed AgNWs and enhance the mechanical robustness of AgNWs network (Figure 4e). Besides, as solvent evaporates, ZnO nanoparticles would tightly aggregate around AgNWs and completely fill into the void space of the grid-like AgNWs network (Figure 4f), leading to a strong bonding of AgNWs to substrate. This also further reduces the impact of brittle ZnO on flexibility.

Distribution of elements of FlexAgNE and FlexAgNE/ZnO stacks provides further evidence for the above mechanism as illustrated in Figure 5b–e and Figure S9, Supporting Information. As characterized by transmission electron microscope (TEM) with energy-dispersive X-ray spectroscopy (EDS), sulfur (S) element from PSSNa distributed homogeneously around Ag atom (from AgNWs), demonstrating that PSSNa tightly surrounds the AgNWs (Figure 5b,c and Figure S9a,b, Supporting Information). Thus, with the strong bonding force between PSSNa and PET as discussed above (Figure 5a), there should be a sufficient force for sticking AgNWs onto PET substrate. In addition, the observed large and uniform existence/distribution of zinc (Zn) element (from ZnO) around AgNWs would offer a strong interaction and bonding between ZnO and FlexAgNE layers in the combined FlexAgNE/ZnO structure (Figure 5d,e and Figure S9c,d, Supporting Information). Consequently, due to all these contributions and the synergistic effect of each component, the combined FlexAgNE/ZnO stacks achieved robust mechanical stability, resulting in the high performance and mechanical robustness of the flexible OPV devices studied in this work.

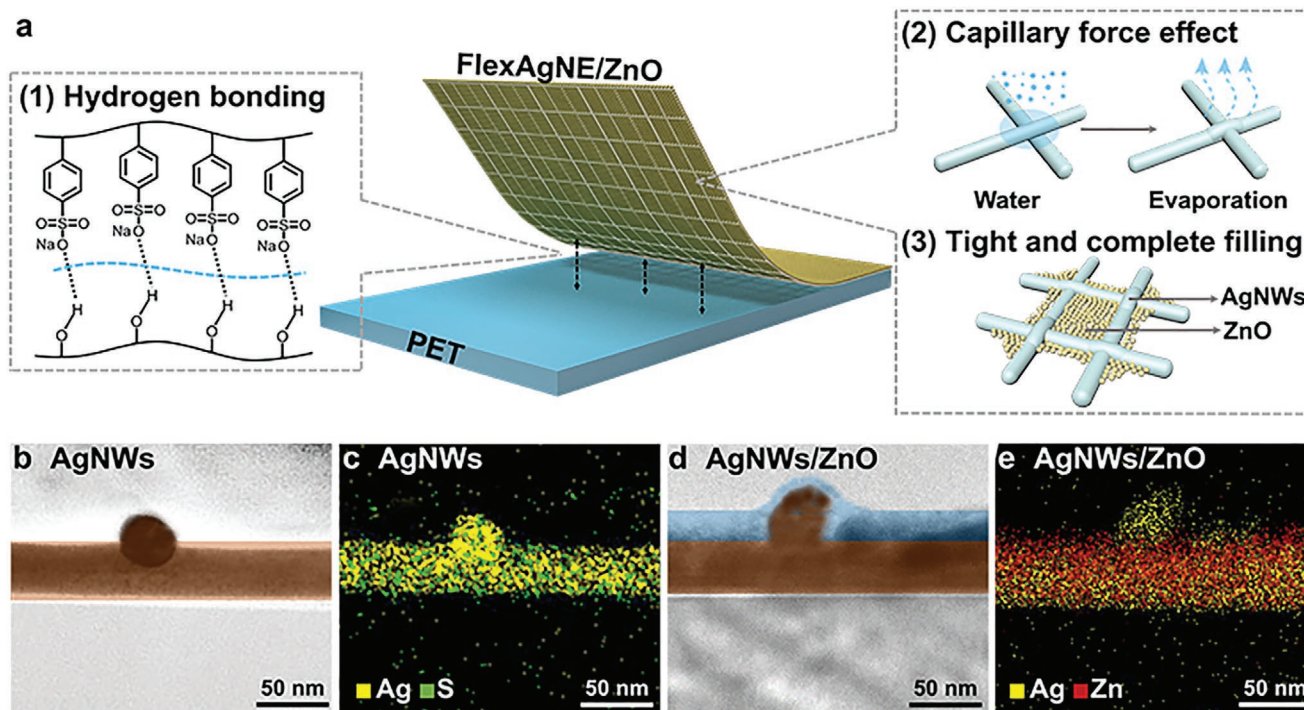


Figure 5. a) Schematic diagram of the mechanism: 1) the hydrogen bond effect between the PET substrate and the hydrophilic polyelectrolyte (PSSNa); 2) the capillary force effect of crossed AgNWs junction, and 3) tight and complete filling of ZnO in grid-like AgNWs network. b) TEM images for the crossed AgNWs junction, which is cut from FlexAgNE using a FIB. c) EDS mapping of the sample in Figure 4b. d) TEM images for the crossed AgNWs junction coated with ZnO (AgNWs/ZnO), which is cut from the FlexAgNE/ZnO stacks using a FIB. e) EDS mapping of the sample in Figure 4d.

3. Conclusion

In summary, based on an easily-prepared high-quality Flex-AgNEs, flexible OPV devices have been fabricated with the newly emerging acceptor Y6 material systems and high performance comparable with rigid counterparts have been demonstrated. In particular, the flexible single-junction devices have offered a high PCE of 15.60%. Also, these flexible devices exhibit robust mechanical stability even under extreme bending or folding conditions. Furthermore, the mechanism underlying the superior mechanical robustness of these flexible devices has been thoroughly investigated for each part, which mainly ascribed to the synergistic effect of FlexAgNEs and the upper ZnO transport layer, including strong bonding of the hydrophilic polyelectrolyte (PSSNa) with PET substrate, along with the capillary force effect of crossed AgNWs and tight filling of ZnO. This comprehensive understanding would guide future high-quality FTEs design for higher and more mechanically stable performance for flexible organic electronics. In light of the aforementioned results, together with our previous report, we anticipate that our FlexAgNEs could successfully be applied for other flexible organic electronics, including light-emitting diodes and field-effect transistors.

Supporting Information

Supporting Information is available from the Wiley Online Library or from the author.

Acknowledgements

Y.S. and L.M. contributed equally to this work. The authors gratefully acknowledge the financial support from Ministry of Science and Technology (2019YFA0705900, 2016YFA0200200) and National Natural Science Foundation of China (21935007, 51873089, 51773095) of China, Tianjin city (20JCZDJC00740 and 17JCJQC44500) and 111 Project (B12015).

Conflict of Interest

The authors declare no conflict of interest.

Data Availability Statement

Research data are not shared.

Keywords

flexible transparent electrodes, mechanical stability, organic photovoltaics, silver nanowires

Received: December 18, 2020

Revised: January 11, 2021

Published online: February 12, 2021

- [1] C. Yan, S. Barlow, Z. Wang, H. Yan, A. K. Y. Jen, S. R. Marder, X. Zhan, *Nat. Rev. Mater.* **2018**, *3*, 18003.
- [2] D. Qian, Z. Zheng, H. Yao, W. Tress, T. R. Hopper, S. Chen, S. Li, J. Liu, S. Chen, J. Zhang, X. K. Liu, B. Gao, L. Ouyang, Y. Jin, G. Pozina, I. A. Buyanova, W. M. Chen, O. Inganas, V. Coropceanu, J. L. Bredas, H. Yan, J. Hou, F. Zhang, A. A. Bakulin, F. Gao, *Nat. Mater.* **2018**, *17*, 703.
- [3] J. Zhang, H. S. Tan, X. Guo, A. Facchetti, H. Yan, *Nat. Energy* **2018**, *3*, 720.
- [4] S. Liu, J. Yuan, W. Deng, M. Luo, Y. Xie, Q. Liang, Y. Zou, Z. He, H. Wu, Y. Cao, *Nat. Photon.* **2020**, *14*, 300.
- [5] X. Wan, C. Li, M. Zhang, Y. Chen, *Chem. Soc. Rev.* **2020**, *49*, 2828.
- [6] L. Meng, Y. Zhang, X. Wan, C. Li, X. Zhang, Y. Wang, X. Ke, Z. Xiao, L. Ding, R. Xia, H. L. Yip, Y. Cao, Y. Chen, *Science* **2018**, *361*, 1094.
- [7] B. Kan, H. Feng, H. Yao, M. Chang, X. Wan, C. Li, J. Hou, Y. Chen, *Sci. China: Chem.* **2018**, *61*, 1307.
- [8] H. Fei, *Acta Polym. Sin.* **2018**, *9*, 1141.
- [9] Y. Cui, H. Yao, J. Zhang, T. Zhang, Y. Wang, L. Hong, K. Xian, B. Xu, S. Zhang, J. Peng, Z. Wei, F. Gao, J. Hou, *Nat. Commun.* **2019**, *10*, 2515.
- [10] Y. Cui, H. Yao, J. Zhang, K. Xian, T. Zhang, L. Hong, Y. Wang, Y. Xu, K. Ma, C. An, C. He, Z. Wei, F. Gao, J. Hou, *Adv. Mater.* **2020**, *32*, 1908205.
- [11] J. Yuan, Y. Zhang, L. Zhou, G. Zhang, H.-L. Yip, T.-K. Lau, X. Lu, C. Zhu, H. Peng, P. A. Johnson, M. Leclerc, Y. Cao, J. Ulanski, Y. Li, Y. Zou, *Joule* **2019**, *3*, 1140.
- [12] R. Yu, H. Yao, Y. Cui, L. Hong, C. He, J. Hou, *Adv. Mater.* **2019**, *31*, 1902302.
- [13] J. Yao, B. Qiu, Z. G. Zhang, L. Xue, R. Wang, C. Zhang, S. Chen, Q. Zhou, C. Sun, C. Yang, M. Xiao, L. Meng, Y. Li, *Nat. Commun.* **2020**, *11*, 2726.
- [14] L. Zhan, S. Li, T.-K. Lau, Y. Cui, X. Lu, M. Shi, C.-Z. Li, H. Li, J. Hou, H. Chen, *Energy Environ. Sci.* **2020**, *13*, 635.
- [15] Q. Liu, Y. Jiang, K. Jin, J. Qin, J. Xu, W. Li, J. Xiong, J. Liu, Z. Xiao, K. Sun, S. Yang, X. Zhang, L. Ding, *Sci. Bull.* **2020**, *65*, 272.
- [16] Y. Lin, B. Adilbekova, Y. Firdaus, E. Yengel, H. Faber, M. Sajjad, X. Zheng, E. Yarali, A. Seitkhan, O. M. Bakr, A. El-Labban, U. Schwingenschlogl, V. Tung, I. McCulloch, F. Laquai, T. D. Anthopoulos, *Adv. Mater.* **2019**, *31*, 1902965.
- [17] Z. Luo, R. Ma, T. Liu, J. Yu, Y. Xiao, R. Sun, G. Xie, J. Yuan, Y. Chen, K. Chen, G. Chai, H. Sun, J. Min, J. Zhang, Y. Zou, C. Yang, X. Lu, F. Gao, H. Yan, *Joule* **2020**, *4*, 1236.
- [18] X. Chen, G. Xu, G. Zeng, H. Gu, H. Chen, H. Xu, H. Yao, Y. Li, J. Hou, Y. Li, *Adv. Mater.* **2020**, *32*, 1908478.
- [19] Z. Jiang, K. Fukuda, W. Huang, S. Park, R. Nur, M. O. G. Nayeem, K. Yu, D. Inoue, M. Saito, H. Kimura, T. Yokota, S. Umez, D. Hashizume, I. Osaka, K. Takimiya, T. Someya, *Adv. Funct. Mater.* **2018**, *29*, 1808378.
- [20] W. Song, B. Fanady, R. Peng, L. Hong, L. Wu, W. Zhang, T. Yan, T. Wu, S. Chen, Z. Ge, *Adv. Energy Mater.* **2020**, *10*, 2000136.
- [21] S. Xiong, L. Hu, L. Hu, L. Sun, F. Qin, X. Liu, M. Fahlman, Y. Zhou, *Adv. Mater.* **2019**, *31*, 1806616.
- [22] K. W. Seo, J. Lee, J. Jo, C. Cho, J. Y. Lee, *Adv. Mater.* **2019**, *31*, 1902447.
- [23] T. Y. Qu, L. J. Zuo, J. D. Chen, X. Shi, T. Zhang, L. Li, K. C. Shen, H. Ren, S. Wang, F. M. Xie, Y. Q. Li, A. K. Y. Jen, J. X. Tang, *Adv. Opt. Mater.* **2020**, 2000669.
- [24] W. Song, X. Fan, B. Xu, F. Yan, H. Cui, Q. Wei, R. Peng, L. Hong, J. Huang, Z. Ge, *Adv. Mater.* **2018**, *30*, 1800075.
- [25] Y. Sun, M. Chang, L. Meng, X. Wan, H. Gao, Y. Zhang, K. Zhao, Z. Sun, C. Li, S. Liu, H. Wang, J. Liang, Y. Chen, *Nat. Electron.* **2019**, *2*, 513.
- [26] K. Fukuda, K. Yu, T. Someya, *Adv. Energy Mater.* **2020**, *10*, 2000765.
- [27] M. Morales-Masis, S. De Wolf, R. Woods-Robinson, J. W. Ager, C. Ballif, *Adv. Electron. Mater.* **2017**, *3*, 1600529.

- [28] M. Vosgueritchian, D. J. Lipomi, Z. Bao, *Adv. Funct. Mater.* **2012**, 22, 421.
- [29] S. Bae, H. Kim, Y. Lee, X. Xu, J. S. Park, Y. Zheng, J. Balakrishnan, T. Lei, H. R. Kim, Y. I. Song, Y. J. Kim, K. S. Kim, B. Ozyilmaz, J. H. Ahn, B. H. Hong, S. Iijima, *Nat. Nanotechnol.* **2010**, 5, 574.
- [30] S. Park, M. Vosgueritchian, Z. Bao, *Nanoscale* **2013**, 5, 1727.
- [31] Y. Li, L. Meng, Y. M. Yang, G. Xu, Z. Hong, Q. Chen, J. You, G. Li, Y. Yang, Y. Li, *Nat. Commun.* **2016**, 7, 10214.
- [32] L. Tan, Y. Wang, J. Zhang, S. Xiao, H. Zhou, Y. Li, Y. Chen, Y. Li, *Adv. Sci.* **2019**, 6, 1801180.
- [33] J. Krantz, T. Stubhan, M. Richter, S. Spallek, I. Litzov, G. J. Matt, E. Spiecker, C. J. Brabec, *Adv. Funct. Mater.* **2013**, 23, 1711.
- [34] Z. Wu, Z. Chen, X. Du, J. M. Logan, J. Sippel, M. Nikolou, K. Kamaras, J. R. Reynolds, D. B. Tanner, A. F. Hebard, A. G. Rinzler, *Science* **2004**, 305, 1273.
- [35] T. Kim, J.-H. Kim, T. E. Kang, C. Lee, H. Kang, M. Shin, C. Wang, B. Ma, U. Jeong, T.-S. Kim, B. J. Kim, *Nat. Commun.* **2015**, 6, 8547.
- [36] Z. Zhao, Q. Liu, W. Zhang, S. Yang, *Sci. China: Chem.* **2018**, 61, 1179.
- [37] M. Hösel, R. R. Søndergaard, M. Jørgensen, F. C. Krebs, *Energy Technol.* **2013**, 1, 102.
- [38] Y. Li, G. Xu, C. Cui, Y. Li, *Adv. Energy Mater.* **2018**, 8, 1701791.
- [39] D. Chen, J. Liang, Q. Pei, *Sci. China: Chem.* **2016**, 59, 659.
- [40] J. Kim, D. Ouyang, H. F. Lu, F. Ye, Y. W. Guo, N. Zhao, W. C. H. Choy, *Adv. Energy Mater.* **2020**, 10, 1903919.
- [41] Z. Yu, L. Li, Q. Zhang, W. Hu, Q. Pei, *Adv. Mater.* **2011**, 23, 4453.
- [42] W. Xiong, H. Liu, Y. Chen, M. Zheng, Y. Zhao, X. Kong, Y. Wang, X. Zhang, X. Kong, P. Wang, L. Jiang, *Adv. Mater.* **2016**, 28, 7167.
- [43] J. H. Seo, I. Hwang, H.-D. Um, S. Lee, K. Lee, J. Park, H. Shin, T.-H. Kwon, S. J. Kang, K. Seo, *Adv. Mater.* **2017**, 29, 1701479.
- [44] L. Hong, H. Yao, Z. Wu, Y. Cui, T. Zhang, Y. Xu, R. Yu, Q. Liao, B. Gao, K. Xian, H. Y. Woo, Z. Ge, J. Hou, *Adv. Mater.* **2019**, 31, 1903441.
- [45] G. Wang, M. A. Adil, J. Zhang, Z. Wei, *Adv. Mater.* **2019**, 31, 1805089.
- [46] I. Lee, J. Noh, J.-Y. Lee, T.-S. Kim, *ACS Appl. Mater. Interfaces* **2017**, 9, 37395.
- [47] L. L. Hench, R. J. Splinter, W. C. Allen, T. K. Greenlee, *J. Biomed. Mater. Res.* **1971**, 5, 117.
- [48] D. Zhang, G. Wang, S. Zhi, K. Xu, L. Zhu, W. Li, Z. Zeng, Q. Xue, *Appl. Surf. Sci.* **2018**, 458, 157.